

Supplementary Information

for

Study on Formation Mechanism and Ligand-directed Architectural Control of Nanoparticles Composed of Bi, Sb and Te: Toward One-pot Synthesis of Ternary (Bi,Sb)₂Te₃ Nanobuilding Blocks

Nguyen T. Mai, Derrick Mott, Nguyen T. B. Thuy, Issey Osaka and Shinya Maenosono

School of Materials Science, Japan Advanced Institute of Science and Technology, 1-1 Asahidai, Nomi, Ishikawa
923-1292, Japan

Table of Contents

1. XRD Peak Assignments	2
1.1. Monometallic Systems	2
1.1.1. Bi monometallic systems	2
1.1.2. Sb monometallic systems	3
1.1.3. Te monometallic systems	4
1.2. Bimetallic Systems	5
1.2.1. Bi-Sb bimetallic systems	5
1.2.2. Bi-Te bimetallic systems	6
1.2.3. Sb-Te bimetallic systems	7
1.3. Trimetallic System	8
2. Monometallic Synthesis of Sb and Te NWs using OAM or OAC/OAM	9
3. Photographs of Metal-Ligand Complexes	10
4. FTICR-MS Spectrum of Sb-DT Complex	10
5. TGA Data of Sb-DT Complex	11
6. HRTEM Image of Bi₇₀Sb₃₀ Alloy NPs	12
7. Relationship between Lattice Spacing and Composition of BiSb Alloy	13
8. Comparison of XRD Peak Position Collected for Resulting NPs Synthesized using BiCl₃ and BiCl₃/SbCl₃ with DT as Capping Ligands	13
9. Bimetallic Synthesis of Bi-Te Halide Precursors and DT	14
10. HRTEM Images of a Single Bi-Sb-Te NW Synthesized using OAM	14
11. Results for Trimetallic Approach using Oleic Acid as Capping System	15

1. XRD Peak Assignments

1.1. Monometallic Systems

1.1.1. Bi monometallic systems

Table S1. XRD peak positions and corresponding crystal planes for Fig. 1A (Bi-OAM system).

2 Theta (Degree)	Intensity	Phase	(<i>h k l</i>)
22.42	Very weak	Bi (RHO)	(0 0 3)
24.16	Strong	BiOCl (TET)	(0 0 2)
25.88	Medium	BiOCl (TET)	(1 0 1)
27.15	Medium	Bi (RHO)	(0 1 2)
32.48	Strong	BiOCl (TET)	(1 1 0)
33.44	Strong	BiOCl (TET)	(1 0 2)
34.73	Very weak	BiOCl (TET)	(1 1 1)
36.56	Medium	BiOCl (TET)	(0 0 3)
38.01	Weak	Bi (RHO)	(1 0 4)
39.70	Weak	Bi (RHO)	(1 1 0)
40.89	Weak	BiOCl (TET)	(1 1 2)
44.53	Very weak	Bi (RHO)	(0 1 5)
45.93	Very weak	Bi (RHO)	(0 0 6)
46.60	Weak	BiOCl (TET)	(2 0 0)
48.36	Very weak	BiOCl (TET)	(2 0 1)
48.76	Very weak	Bi (RHO)	(2 0 2)
49.62	Weak	BiOCl (TET)	(1 1 3)
53.06	Very weak	BiOCl (TET)	(2 0 2)
54.04	Weak	BiOCl (TET)	(2 1 1)
55.14	Weak	BiOCl (TET)	(1 0 4)
58.56	Weak	BiOCl (TET)	(2 1 2)

RHO=Rhombohedral, TET=Tetragonal

Table S2. XRD peak positions and corresponding crystal planes for Fig. 1B (Bi-OAC/OAM system).

2 Theta (Degree)	Intensity	Phase	(<i>h k l</i>)
24.10	Strong	BiOCl (TET)	(0 0 2)
25.78	Weak	BiOCl (TET)	(1 0 1)
27.16	Weak	Bi (RHO)	(0 1 2)
32.50	Medium	BiOCl (TET)	(1 1 0)
33.40	Medium	BiOCl (TET)	(1 0 2)
34.76	Very weak	BiOCl (TET)	(1 1 1)
36.54	Strong	BiOCl (TET)	(0 0 3)
37.96	Weak	Bi (RHO)	(1 0 4)
39.54	Weak	Bi (RHO)	(1 1 0)
40.88	Weak	BiOCl (TET)	(1 1 2)
44.60	Very weak	Bi (RHO)	(0 1 5)
45.90	Very weak	Bi (RHO)	(0 0 6)
46.60	Weak	BiOCl (TET)	(2 0 0)
48.34	Very weak	BiOCl (TET)	(2 0 1)
49.56	Weak	BiOCl (TET)	(1 1 3)
53.16	Very weak	BiOCl (TET)	(2 0 2)
54.10	Weak	BiOCl (TET)	(2 1 1)
55.02	Weak	BiOCl (TET)	(1 0 4)
58.56	Weak	BiOCl (TET)	(2 1 2)

RHO=Rhombohedral, TET=Tetragonal

Table S3. XRD peak positions and corresponding crystal planes for Fig. 1C (Bi-DT system).

2 Theta (Degree)	Intensity	Phase	(h k l)
22.44	Very weak	Bi (RHO)	(0 0 3)
23.81	Very weak	Bi (RHO)	(1 0 1)
27.12	Strong	Bi (RHO)	(0 1 2)
37.92	Medium	Bi (RHO)	(1 0 4)
39.59	Medium	Bi (RHO)	(1 1 0)
44.53	Very weak	Bi (RHO)	(0 1 5)
45.95	Very weak	Bi (RHO)	(0 0 6)
46.89	Very weak	Bi (RHO)	(0 2 1)
48.66	Weak	Bi (RHO)	(2 0 2)
55.97	Very weak	Bi (RHO)	(0 2 4)
59.29	Very weak	Bi (RHO)	(1 0 7)

RHO=Rhombohedral

1.1.2. Sb monometallic systems

Table S4. XRD peak positions and corresponding crystal planes for Fig. 2A (Sb-OAM system).

2 Theta (Degree)	Intensity	Phase	(h k l)
23.66	Very weak	Sb (RHO)	(0 0 3)
28.65	Strong	Sb (RHO)	(0 1 2)
39.98	Weak	Sb (RHO)	(1 0 4)
41.88	Weak	Sb (RHO)	(1 1 0)
46.98	Very weak	Sb (RHO)	(0 1 5)
48.41	Very weak	Sb (RHO)	(0 0 6)
51.54	Very weak	Sb (RHO)	(2 0 2)
59.39	Very weak	Sb (RHO)	(0 2 4)

RHO=Rhombohedral

Table S5. XRD peak positions and corresponding crystal planes for Fig. 2B (Sb-OAC/OAM system).

2 Theta (Degree)	Intensity	Phase	(h k l)
23.64	Very weak	Sb (RHO)	(0 0 3)
28.62	Strong	Sb (RHO)	(0 1 2)
40.00	Medium	Sb (RHO)	(1 0 4)
41.91	Medium	Sb (RHO)	(1 1 0)
47.09	Very weak	Sb (RHO)	(0 1 5)
48.35	Very weak	Sb (RHO)	(0 0 6)
51.50	Weak	Sb (RHO)	(2 0 2)
59.33	Very weak	Sb (RHO)	(0 2 4)

RHO=Rhombohedral

1.1.3. Te monometallic systems

Table S6. XRD peak positions and corresponding crystal planes for Fig. 3A (Te-OAM system).

2 Theta (Degree)	Intensity	Phase	(h k l)
23.00	Weak	Te (HEX)	(1 0 0)
27.52	Strong	Te (HEX)	(1 0 1)
38.22	Medium	Te (HEX)	(1 0 2)
40.41	Medium	Te (HEX)	(1 1 0)
43.36	Very weak	Te (HEX)	(1 1 1)
45.97	Very weak	Te (HEX)	(0 0 3)
47.12	Very weak	Te (HEX)	(2 0 0)
49.62	Weak	Te (HEX)	(2 0 1)
51.22	Very weak	Te (HEX)	(1 1 2)
51.93	Very weak	Te (HEX)	(1 0 3)
56.83	Very weak	Te (HEX)	(2 0 2)

HEX=Hexagonal

Table S7. XRD peak positions and corresponding crystal planes for Fig. 3B (Te-OAC/OAM system).

2 Theta (Degree)	Intensity	Phase	(h k l)
23.00	Weak	Te (HEX)	(1 0 0)
27.52	Strong	Te (HEX)	(1 0 1)
38.24	Weak	Te (HEX)	(1 0 2)
40.42	Weak	Te (HEX)	(1 1 0)
43.36	Very weak	Te (HEX)	(1 1 1)
45.88	Very weak	Te (HEX)	(0 0 3)
47.12	Very weak	Te (HEX)	(2 0 0)
49.62	Very weak	Te (HEX)	(2 0 1)
51.24	Very weak	Te (HEX)	(1 1 2)
52.04	Very weak	Te (HEX)	(1 0 3)
56.84	Very weak	Te (HEX)	(2 0 2)

HEX=Hexagonal

Table S8. XRD peak positions and corresponding crystal planes for Fig. 3C (Te-DT system).

2 Theta (Degree)	Intensity	Phase	(h k l)
23.00	Weak	Te (HEX)	(1 0 0)
27.54	Strong	Te (HEX)	(1 0 1)
38.24	Medium	Te (HEX)	(1 0 2)
40.46	Weak	Te (HEX)	(1 1 0)
43.42	Very weak	Te (HEX)	(1 1 1)
46.04	Very weak	Te (HEX)	(0 0 3)
47.16	Very weak	Te (HEX)	(2 0 0)
49.68	Very weak	Te (HEX)	(2 0 1)
51.24	Very weak	Te (HEX)	(1 1 2)
52.06	Very weak	Te (HEX)	(1 0 3)
56.88	Very weak	Te (HEX)	(2 0 2)

HEX=Hexagonal

1.2. Bimetallic Systems

1.2.1. Bi-Sb bimetallic systems

Table S9. XRD peak positions and corresponding crystal planes for Fig. 4A (Bi/Sb-OAM system).

2 Theta (Degree)	Intensity	Phase	(<i>h k l</i>)
27.45	Strong	BiSb (RHO)	(0 1 2)
38.34	Weak	BiSb (RHO)	(1 0 4)
40.33	Medium	BiSb (RHO)	(1 1 0)
46.34	Very weak	BiSb (RHO)	(0 1 5)
49.44	Very weak	BiSb (RHO)	(2 0 2)
56.78	Very weak	BiSb (RHO)	(0 2 4)

RHO=Rhombohedral

Table S10. XRD peak positions and corresponding crystal planes for Fig. 4B (Bi/Sb-OAC/OAM system).

2 Theta (Degree)	Intensity	Phase	(<i>h k l</i>)
22.54	Very weak	BiSb (RHO)	(0 0 3)
27.28	Strong	BiSb (RHO)	(0 1 2)
38.14	Weak	BiSb (RHO)	(1 0 4)
39.78	Medium	BiSb (RHO)	(1 1 0)
44.78	Very weak	Bi (RHO)	(0 1 5)
46.12	Very weak	BiSb (RHO)	(0 1 5)
48.96	Very weak	BiSb (RHO)	(2 0 2)
56.28	Very weak	BiSb (RHO)	(0 2 4)

RHO=Rhombohedral

Table S11. XRD peak positions and corresponding crystal planes for Fig. 4C (Bi/Sb-DT system).

2 Theta (Degree)	Intensity	Phase	(<i>h k l</i>)
22.32	Weak	Bi (RHO)	(0 0 3)
23.60	Very weak	Bi (RHO)	(1 0 1)
27.14	Strong	Bi (RHO)	(0 1 2)
37.92	Medium	Bi (RHO)	(1 0 4)
39.60	Medium	Bi (RHO)	(1 1 0)
44.56	Very weak	Bi (RHO)	(0 1 5)
45.18	Very weak	Bi (RHO)	(0 0 6)
45.90	Very weak	Bi (RHO)	(1 1 3)
46.74	Very weak	Bi (RHO)	(0 2 1)
48.66	Very weak	Bi (RHO)	(2 0 2)
56.02	Very weak	Bi (RHO)	(0 2 4)
59.30	Very weak	Bi (RHO)	(1 0 7)

RHO=Rhombohedral

1.2.2. Bi-Te bimetallic systems

Table S12. XRD peak positions and corresponding crystal planes for Fig. 5A (Bi/Te-OAM system).

2 Theta (Degree)	Intensity	Phase	(h k l)
23.01	Weak	Te (HEX)	(1 0 0)
27.56	Strong	Te (HEX)	(1 0 1)
38.31	Very weak	Te (HEX)	(1 0 2)
40.34	Medium	Te (HEX)	(1 1 0)
43.36	Very weak	Te (HEX)	(1 1 1)
45.88	Very weak	Te (HEX)	(0 0 3)
47.02	Very weak	Te (HEX)	(2 0 0)
49.57	Weak	Te (HEX)	(2 0 1)
51.42	Very weak	Te (HEX)	(1 1 2)
56.91	Very weak	Te (HEX)	(2 0 2)

HEX=Hexagonal

Table S13. XRD peak positions and corresponding crystal planes for Fig. 5B (Bi/Te-OAC/OAM system).

2 Theta (Degree)	Intensity	Phase	(h k l)
23.02	Weak	Te (HEX)	(1 0 0)
27.54	Strong	Te (HEX)	(1 0 1)
38.28	Weak	Te (HEX)	(1 0 2)
40.40	Weak	Te (HEX)	(1 1 0)
43.38	Very weak	Te (HEX)	(1 1 1)
45.98	Very weak	Te (HEX)	(0 0 3)
47.16	Very weak	Te (HEX)	(2 0 0)
49.62	Weak	Te (HEX)	(2 0 1)
51.26	Very weak	Te (HEX)	(1 1 2)
52.08	Very weak	Te (HEX)	(1 0 3)
56.86	Very weak	Te (HEX)	(2 0 2)

HEX=Hexagonal

Table S14. XRD peak positions and corresponding crystal planes for Fig. 5C (Bi/Te-DT system).

2 Theta (Degree)	Intensity	Phase	(h k l)
23.60	Very weak	Bi ₂ Te ₃ (RHO)	(1 0 1)
27.62	Strong	Bi ₂ Te ₃ (RHO)	(0 1 5)
37.96	Weak	Bi ₂ Te ₃ (RHO)	(1 0 10)
40.38	Very weak	Bi ₂ Te ₃ (RHO)	(0 1 11)
41.16	Weak	Bi ₂ Te ₃ (RHO)	(1 1 0)
44.68	Very weak	Bi ₂ Te ₃ (RHO)	(0 0 15)
45.00	Very weak	Bi ₂ Te ₃ (RHO)	(1 1 6)
50.32	Very weak	Bi ₂ Te ₃ (RHO)	(2 0 5)
54.02	Very weak	Bi ₂ Te ₃ (RHO)	(0 0 18)
57.18	Very weak	Bi ₂ Te ₃ (RHO)	(0 2 10)

RHO=Rhombohedral

1.2.3. Sb-Te bimetallic systems

Table S15. XRD peak positions and corresponding crystal planes for Fig. 6A (Sb/Te-OAM system).

2 Theta (Degree)	Intensity	Phase	(h k l)
22.94	Weak	Te (HEX)	(1 0 0)
27.43	Strong	Te (HEX)	(1 0 1)
38.15	Weak	Te (HEX)	(1 0 2)
40.37	Strong	Te (HEX)	(1 1 0)
43.18	Weak	Te (HEX)	(1 1 1)
45.87	Very weak	Te (HEX)	(0 0 3)
47.02	Very weak	Te (HEX)	(2 0 0)
49.49	Medium	Te (HEX)	(2 0 1)
51.22	Very weak	Te (HEX)	(1 1 2)
51.93	Very weak	Te (HEX)	(1 0 3)
56.72	Weak	Te (HEX)	(2 0 2)

HEX=Hexagonal

Table S16. XRD peak positions and corresponding crystal planes for Fig. 6B (Sb/Te-OAC/OAM system).

2 Theta (Degree)	Intensity	Phase	(h k l)
23.00	Weak	Te (HEX)	(1 0 0)
27.54	Strong	Te (HEX)	(1 0 1)
38.26	Weak	Te (HEX)	(1 0 2)
40.42	Medium	Te (HEX)	(1 1 0)
43.34	Very weak	Te (HEX)	(1 1 1)
45.88	Very weak	Te (HEX)	(0 0 3)
47.06	Very weak	Te (HEX)	(2 0 0)
49.62	Weak	Te (HEX)	(2 0 1)
51.24	Very weak	Te (HEX)	(1 1 2)
52.04	Very weak	Te (HEX)	(1 0 3)
56.86	Very weak	Te (HEX)	(2 0 2)

HEX=Hexagonal

Table S17. XRD peak positions and corresponding crystal planes for Fig. 6C (Sb/Te-DT system).

2 Theta (Degree)	Intensity	Phase	(h k l)
23.00	Very weak	Te (HEX)	(1 0 0)
26.32	Very weak	Sb ₂ Te ₃ (RHO)	(0 0 9)
26.80	Very weak	Sb ₂ Te ₃ (RHO)	(1 0 4)
27.54	Weak	Te (HEX)	(1 0 1)
28.20	Strong	Sb ₂ Te ₃ (RHO)	(0 1 5)
31.70	Very weak	Sb ₂ Te ₃ (RHO)	(1 0 7)
33.80	Very weak	Sb ₂ Te ₃ (RHO)	(0 1 8)
38.26	Medium	Sb ₂ Te ₃ (RHO), Te (HEX)	(1 0 10), (1 0 2)
40.42	Very weak	Te (HEX)	(1 1 0)
40.70	Very weak	Sb ₂ Te ₃ (RHO)	(0 1 11)
42.30	Weak	Sb ₂ Te ₃ (RHO)	(1 1 0)
43.32	Very weak	Te (HEX)	(1 1 1)
44.58	Very weak	Sb ₂ Te ₃ (RHO)	(0 0 15)
45.94	Very weak	Sb ₂ Te ₃ (RHO), Te (HEX)	(1 0 13), (0 0 3)
48.54	Very weak	Sb ₂ Te ₃ (RHO)	(0 1 14)
49.60	Very weak	Te (HEX)	(2 0 1)
50.56	Very weak	Sb ₂ Te ₃ (RHO)	(1 1 9)
51.64	Very weak	Sb ₂ Te ₃ (RHO)	(2 0 5)
54.20	Very weak	Sb ₂ Te ₃ (RHO)	(0 0 18)
56.86	Very weak	Sb ₂ Te ₃ (RHO), Te (HEX)	(0 1 17), (2 0 2)
58.36	Very weak	Sb ₂ Te ₃ (RHO)	(0 2 10)

HEX=Hexagonal, RHO=Rhombohedral

1.3. Trimetallic System

Table S18. XRD peak positions and corresponding crystal planes for Fig. 8 (Bi/Sb/Te-OAM system).

2 Theta (Degree)	Intensity	Phase	(<i>h k l</i>)
22.98	Very weak	Te (HEX)	(1 0 0)
23.56	Very weak	BiSbTe (RHO)	(1 0 1)
27.59	Strong	Te (HEX), BiSbTe (RHO)	(1 0 1), (0 1 5)
33.27	Very weak	BiSbTe (RHO)	(0 1 8)
37.73	Medium	BiSbTe (RHO)	(1 0 10)
38.21	Weak	Te (HEX)	(1 0 2)
40.38	Weak	Te (HEX)	(1 1 0)
41.11	Medium	BiSbTe (RHO)	(1 1 0)
43.28	Very weak	Te (HEX)	(1 1 1)
44.46	Very weak	BiSbTe (RHO)	(0 0 15)
44.95	Very weak	BiSbTe (RHO)	(1 1 6)
45.44	Very weak	BiSbTe (RHO)	(1 0 13)
45.86	Very weak	Te (HEX)	(0 0 3)
49.55	Very weak	Te (HEX)	(2 0 1)
50.27	Weak	BiSbTe (RHO)	(2 0 5)
51.16	Very weak	Te (HEX)	(1 1 2)
51.92	Very weak	Te (HEX)	(1 0 3)
53.74	Very weak	BiSbTe (RHO)	(1 0 16)
56.84	Very weak	Te (HEX)	(2 0 2)
57.05	Weak	BiSbTe (RHO)	(0 2 10)
58.95	Very weak	BiSbTe (RHO)	(2 0 11)
62.17	Weak	BiSbTe (RHO)	(1 1 15)
62.76	Very weak	BiSbTe (RHO)	(0 2 13)
63.66	Very weak	BiSbTe (RHO)	(0 0 21)
65.90	Weak	BiSbTe (RHO)	(0 1 20)
66.88	Weak	BiSbTe (RHO)	(1 2 5)
67.65	Very weak	Te (HEX)	(1 0 4)
70.09	Very weak	BiSbTe (RHO)	(0 2 16)
72.08	Very weak	Te (HEX)	(2 1 2)
72.68	Weak	BiSbTe (RHO)	(2 1 10)
74.91	Very weak	BiSbTe (RHO)	(1 2 11)
77.87	Very weak	Te (HEX)	(1 1 4)
79.03	Very weak	BiSbTe (RHO)	(1 1 21)

HEX=Hexagonal, RHO=Rhombohedral

2. Monometallic Synthesis of Sb and Te NWs using OAM or OAC/OAM

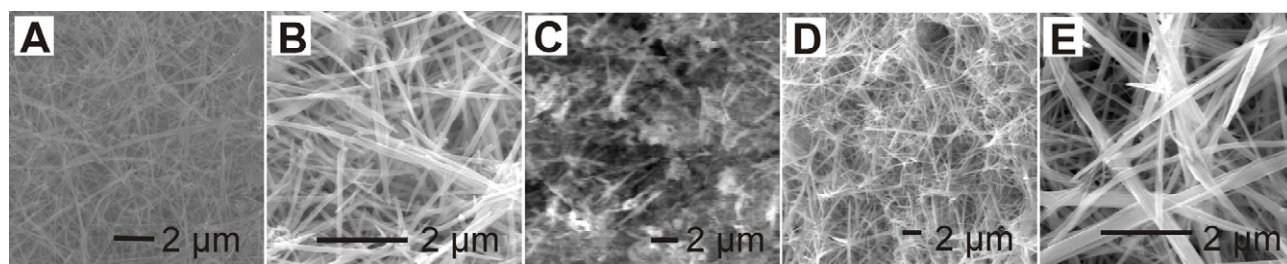


Figure S1. SEM images of (A and B) Sb NWs synthesized using OAM, (C) Sb NWs synthesized using OAC/OAM, and (D and E) Te NWs synthesized using OAM.

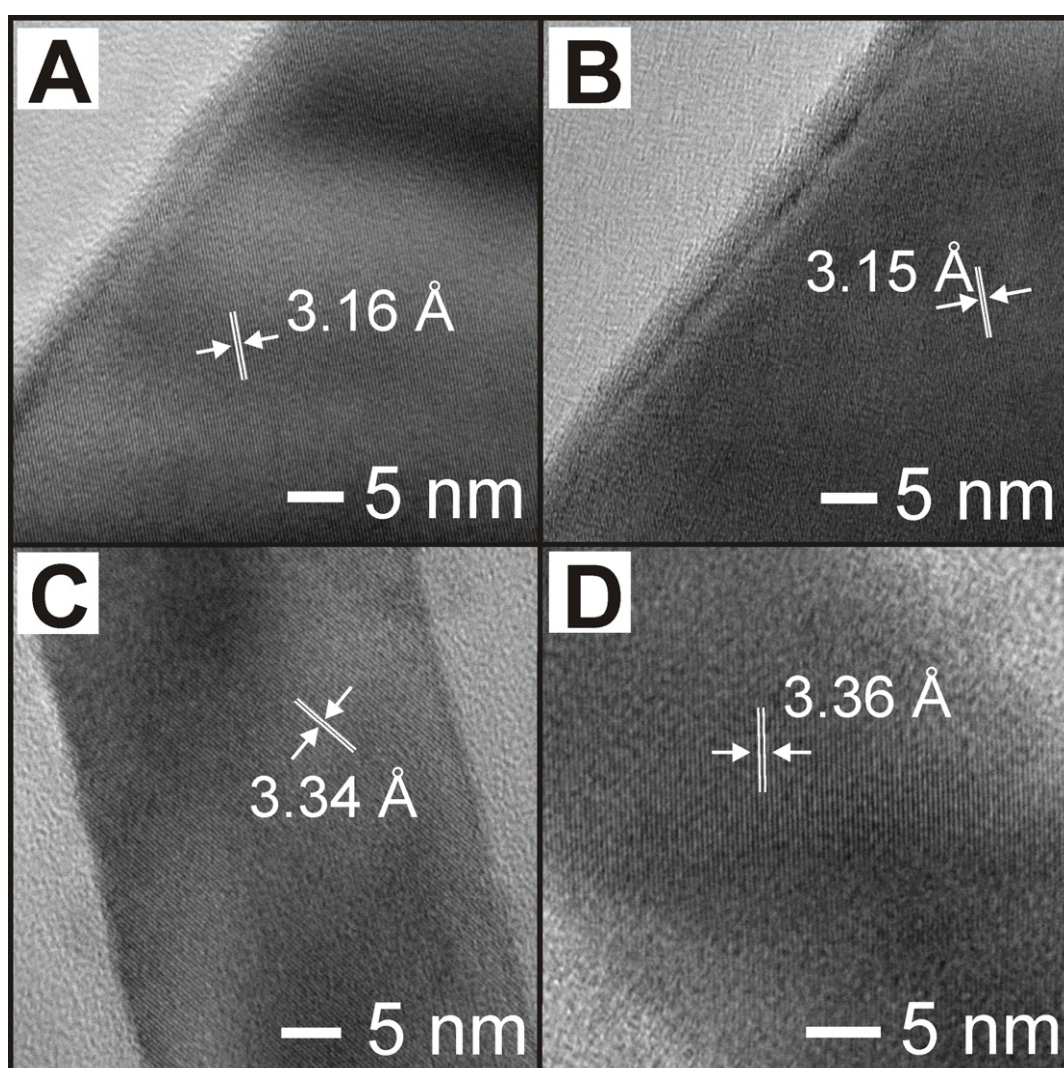


Figure S2. (A and B) HRTEM images of different parts of a single Sb NW synthesized using OAM. Lattice fringes indicated in the images correspond to the (012) plane of rhombohedral Sb. (C and D) HRTEM images of a single Te NW synthesized using OAM. Lattice fringes correspond to the (101) plane of hexagonal Te.

3. Photographs of Metal-Ligand Complexes

Each elemental precursor was dissolved in hexane solvent with a single capping ligand including OAM, OAC or DT under nitrogen atmosphere followed by stirring for 24 hours at room temperature. After that, a filter was used to separate the solid precursor from the liquid complex solution for analysis. The complexes of elemental precursors and each capping ligand have a different color as shown in Fig. S3.

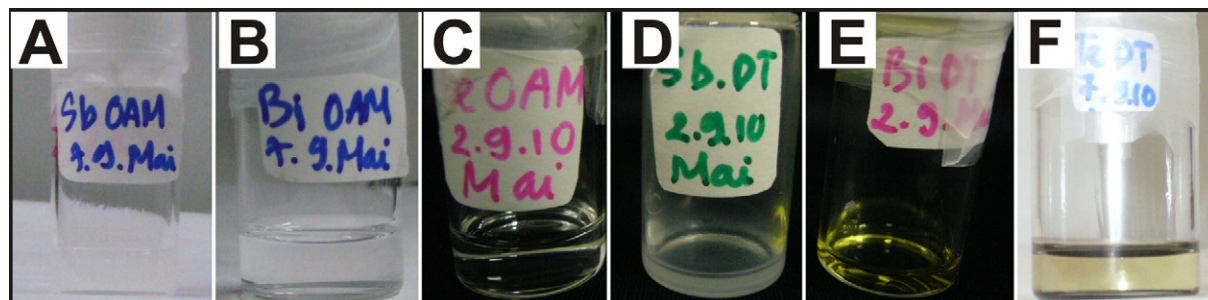


Figure S3. Photographs of single elemental complex solutions of Sb, Bi and Te with OAM and DT capping ligands. (A) Sb-OAM, (B) Bi-OAM, (C) Te-OAM, (D) Sb-DT, (E) Bi-DT and (F) Te-DT.

4. FTICR-MS Spectrum of Sb-DT Complex

To prove the existence of the metal-ligand complex, we conducted electrospray ionization Fourier transform ion cyclotron resonance mass spectroscopy (ESI-FTICR-MS) analysis for the Sb-DT complex. A Fourier transform ion cyclotron resonance mass spectrometer (FTICR-MS) equipped with a 9.4 T superconducting magnet (Solarix, Bruker Daltonics) was used for the analysis of the sample solutions. MS detection was performed in positive-ion ESI mode. Since Sb-DT complexes are thought to be relatively stable and Sb(III) shows specific isotope patterns (^{121}Sb : ^{123}Sb ; 57:43), they can easily be recognized in the mass spectrum.

Figure S4 shows an averaged mass spectrum measured for the sample prepared by dissolving SbCl_3 in DT at a concentration of 1×10^{-3} mM followed by dilution using 2-propanol. The spectrum shows various ions which are not observed for pure DT at an m/z range of 600-700. Two intense peaks are observed at m/z 611.32091 and 647.29856.

First, we analyzed the peak at m/z 611.32091 (Peak611) and its satellite peaks. The difference in m/z between the peak at m/z 613.32102 (Peak613) and Peak611 exactly corresponds to the difference in accurate mass numbers of the stable isotopes of Sb. In addition, the intensity ratio between Peak611 and Peak613 is close to the isotope abundance ratio. The accurate mass obtained with the FTICR-MS supports the identification of Sb.

On the other hand, the difference in m/z between the peak at m/z 612.32340 (or m/z 614.32305) and Peak611 (or Peak613) exactly corresponds to the difference in accurate mass numbers of the stable isotopes of C ($^{12}\text{C}=12$, $^{13}\text{C}=13.00335484$). This result indicates that the ion has a molecular structure that contains carbon atoms. Consequently, we can conclude that Peak611 corresponds to a specific ion related to an Sb-DT complex, even though we couldn't identify its composition.

Therefore, the Peak611 is designated as $[^{121}\text{Sb}_x\text{Y}]^+$ hereafter where Y represents a DT-derived organic ligand.

Next, the peak at m/z 647.29856 (Peak647) and its satellite peaks are investigated. Again, the difference in m/z between Peak647 and the peak at m/z 649.29791 (Peak649) exactly corresponds to the difference in accurate mass numbers of the stable isotopes of Sb. Also, the difference in m/z between the peak at m/z 648.30152 (or m/z 650.29976) and Peak647 (or Peak649) exactly corresponds to the difference in accurate mass numbers of the stable isotopes of C. Thus, we can conclude that Peak647 also corresponds to another ion related to an Sb-DT complex, which has a different ligand structure compared to $[^{121}\text{Sb}_x\text{Y}]^+$. Thus, the Peak647 is designated as $[^{121}\text{Sb}_x\text{Z}]^+$ where Z represents a DT-derived organic ligand whose molecular structure differs from Y.

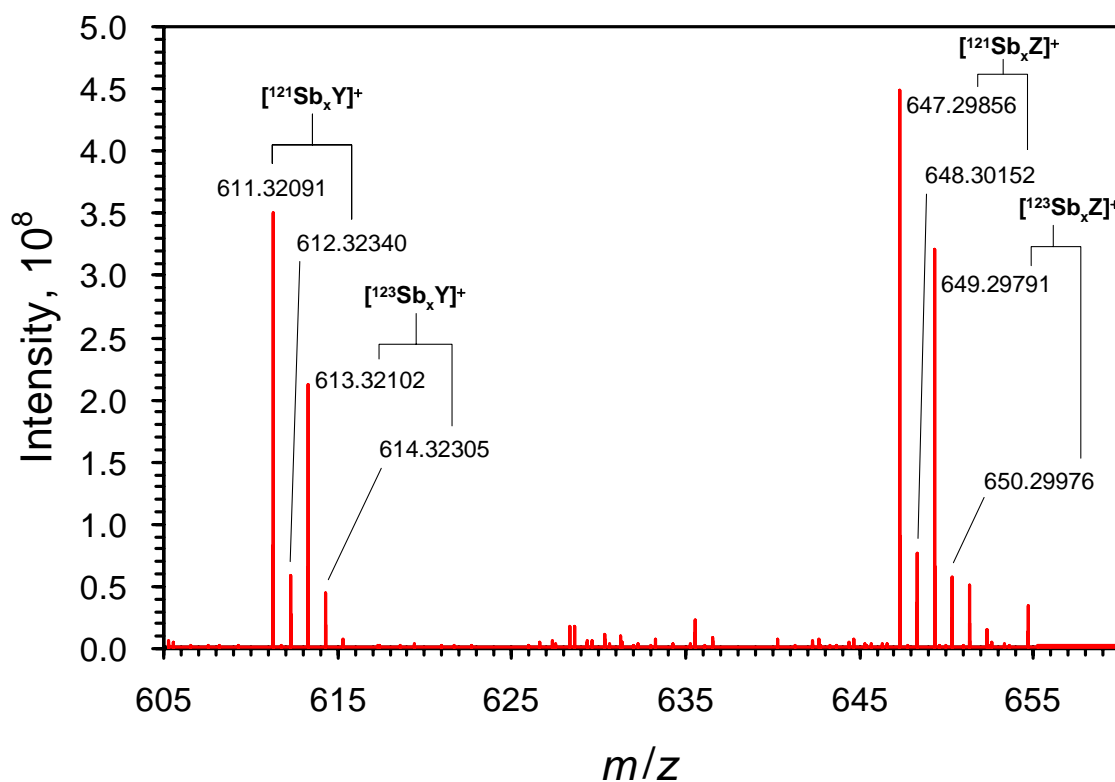


Figure S4. ESI-FTICR-MS spectrum of Sb-DT complexes.

5. TGA Data of Sb-DT Complex

Thermogravimetric analysis (TGA) was performed using a Seiko TG/DTA6200 to investigate the thermal decomposition behavior of the Sb-DT complex. 39.618 milligrams of the Sb-DT complex was placed in an aluminum pan, and this was then placed in the TGA instrument. The temperature was raised to 600 °C at a heating rate of 10 °C/min under a N₂ atmosphere (flow rate 200 mL/min). Figure S5 shows the resulting TG curve for the analysis of the Sb-DT complex.

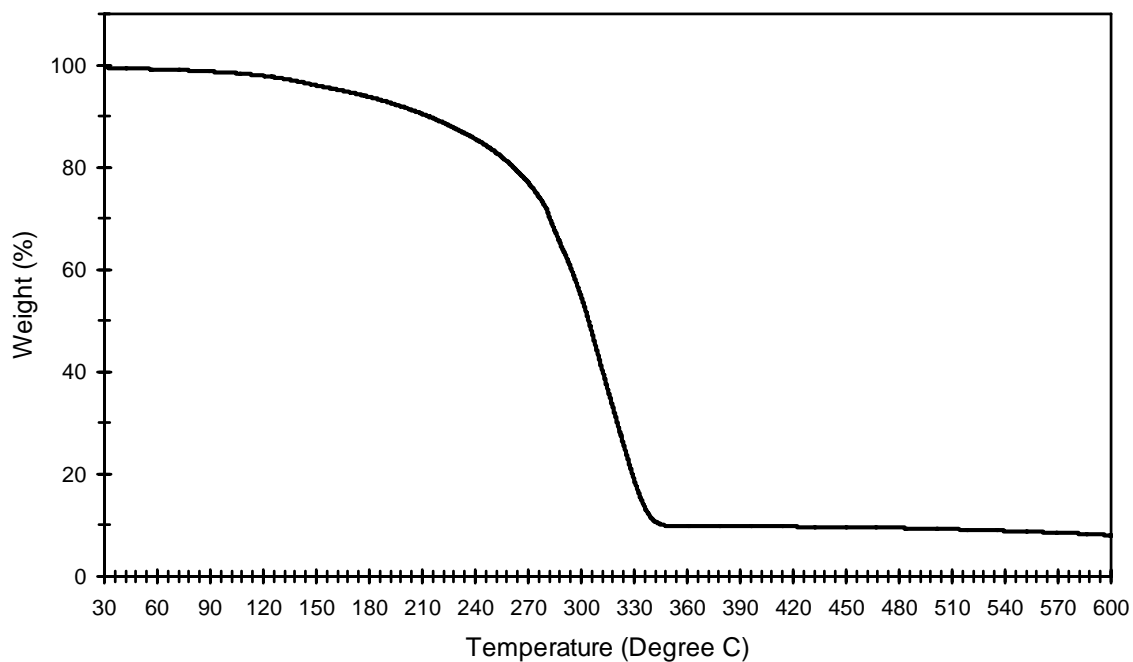


Figure S5. TG curve of Sb-DT complex.

6. HRTEM image of Bi₇₀Sb₃₀ Alloy NPs

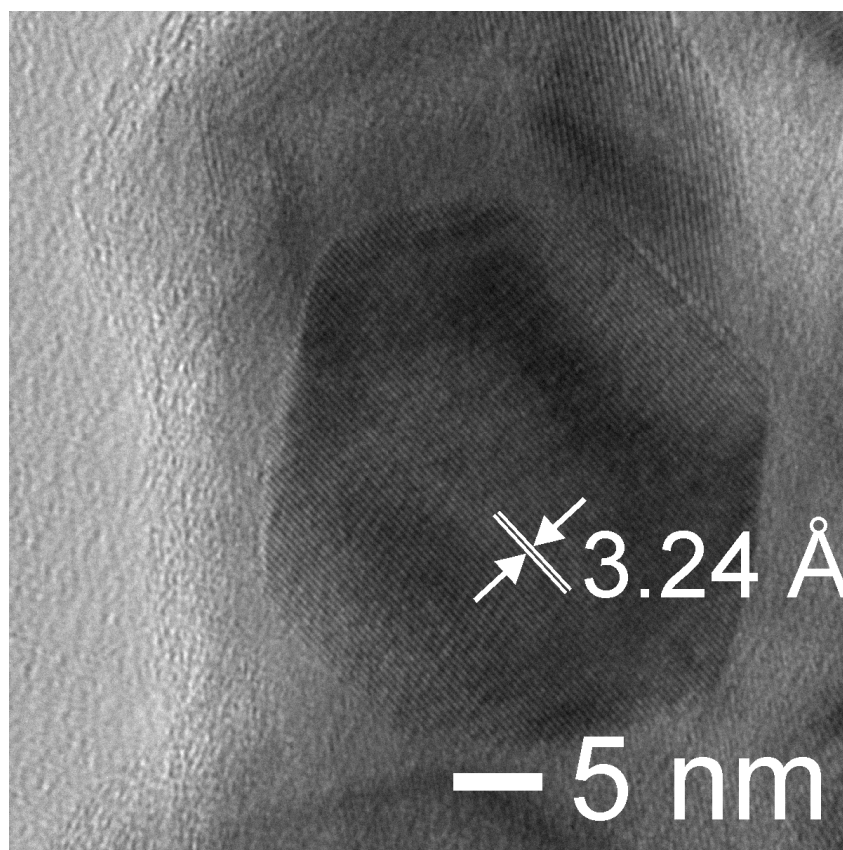


Figure S6. HRTEM image of a single Bi₇₀Sb₃₀ NP synthesized using OAM as capping ligand. The lattice spacing measured is 3.24 Å which corresponds to the (012) crystal plane of Bi₇₀Sb₃₀ alloy.

7. Relationship between Lattice Spacing and Composition of BiSb Alloy

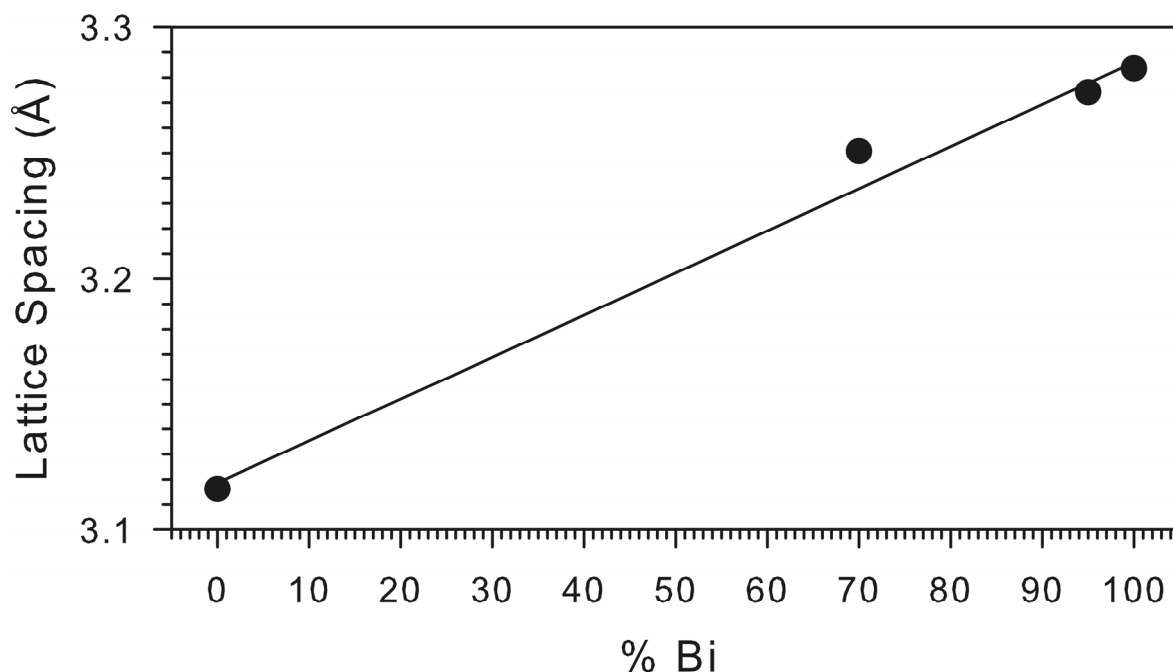


Figure S7. Relationship between the lattice spacing of (012) crystal plane and composition of BiSb alloy synthesized based on bimetallic approach using OAM ($\text{Bi}_{70}\text{Sb}_{30}$) and OAC/OAM ($\text{Bi}_{95}\text{Sb}_5$). The lattice distance of crystal plane (012) of pure Bi, Sb and BiSb alloy were calculated based on XRD peak positions of (012) crystal plane collected for the corresponding synthesized NPs. The Williamson-Hall plot analysis was also conducted to exclude the strain broadening contribution. As a result, it is found that the strain component is negligibly small ensuring that the Vegard's law can be quantitatively applied.

8. Comparison of XRD Peak Position Collected for Resulting NPs Synthesized using BiCl_3 and $\text{BiCl}_3/\text{SbCl}_3$ with DT as Capping Ligands

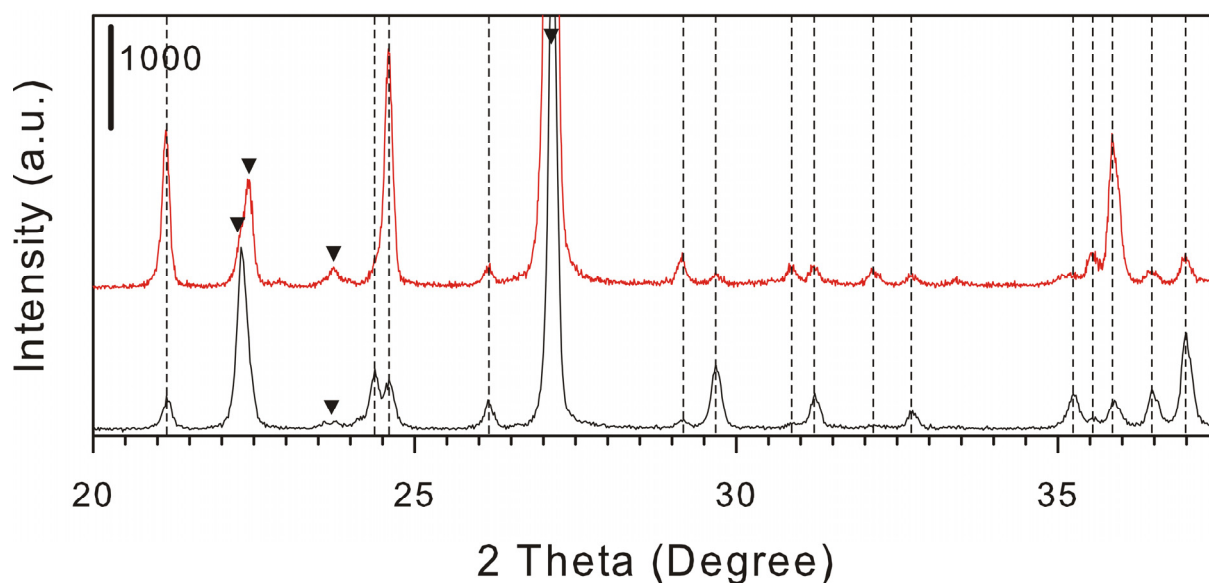


Figure S8. XRD patterns of NPs synthesized using DT and BiCl_3 (red curve) and $\text{BiCl}_3/\text{SbCl}_3$ (black curve) in range of 20 to 37.5 in two theta degree. The symbol (▼) was used to label for the peaks of Bi with rhombohedral structure. The unidentifiable peaks for these two NPs are found to have the same pattern. The dash lines were used to show the coincidence of the unidentifiable peak position of those two XRD patterns.

9. Bimetallic Synthesis of Bi-Te Halide Precursors and DT

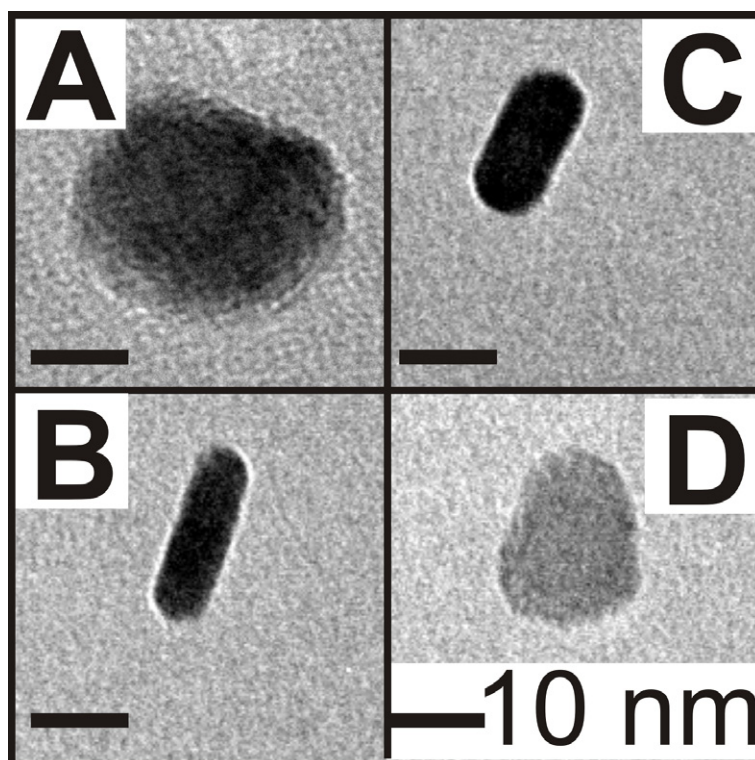


Figure S9. TEM images for NPs synthesized using Bi-Te halide precursors and DT as capping species. The images of individual NPs show the different contrast arising from the different alignment with electron beam in which (A and D) show the top down view and (B and C) show the side view of disc like NPs.

10. HRTEM Images of a Single Bi-Sb-Te NW Synthesized using OAM

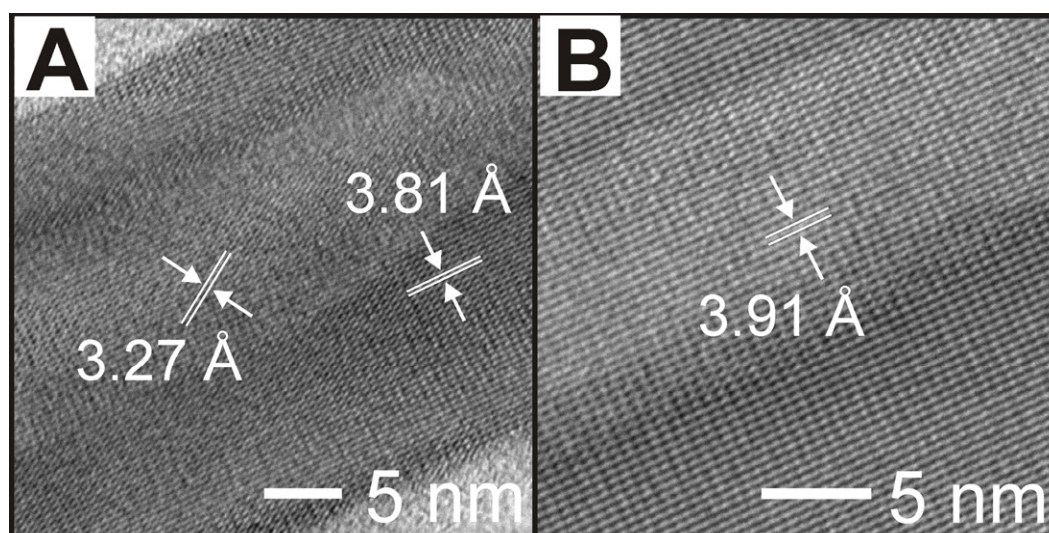


Figure S10. HRTEM images of different parts of a single Bi-Sb-Te NW synthesized using OAM.

11. Results for Trimetallic Approach using Oleic Acid as Capping System

The resulting NPs obtained for trimetallic synthesis using oleic acid as capping species shows NDs studded on NWs in the TEM images (Fig. S11). The XRD pattern collected for these materials shows the existence of several phases including Te, Bi₂Te₃ and Sb₂Te₃ (Fig. S12). The elemental analysis based on ICP-MS confirmed the composition of Bi₁₁Sb₂₃Te₆₆ which is consistent with the XRD results.

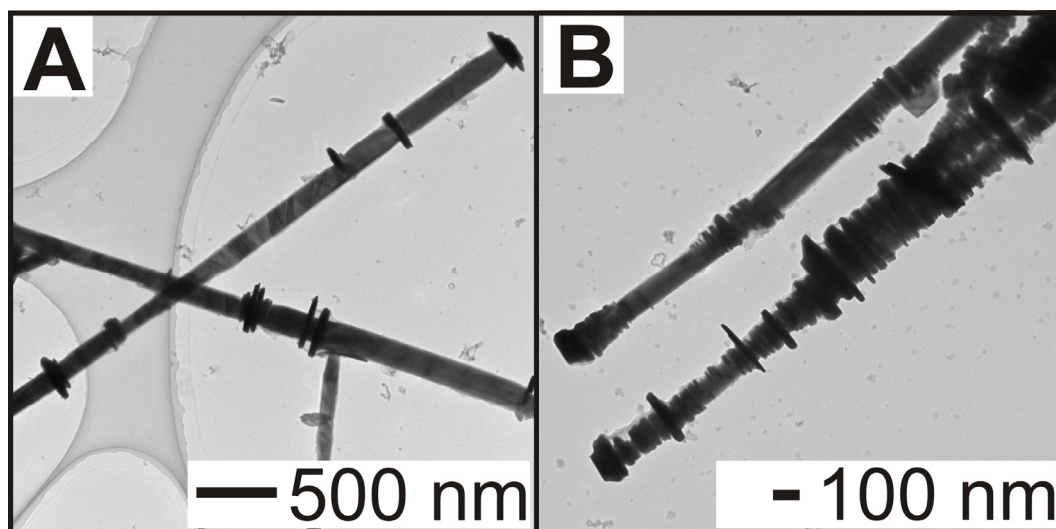


Figure S11. TEM images for NPs synthesized using three elemental precursors and OAC as capping species with 1:1 molar ratio between precursors and OAC.

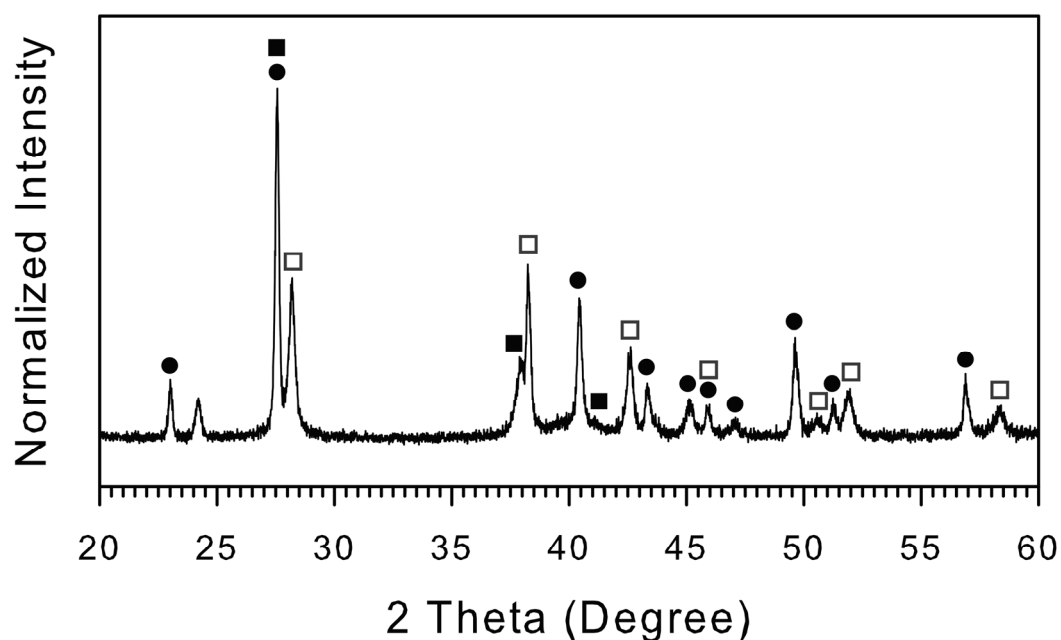


Figure S12. XRD pattern for resulting NPs synthesized using three elemental precursors and OAC as capping species with 1:1 molar ratio between precursors and OAC. The peak identities were label by symbol circle (●) for hexagonal Te, filled square (■) for rhombohedral Bi₂Te₃ and open square (□) for rhombohedral Sb₂Te₃.

Table S19. XRD peak positions and corresponding crystal planes for Fig. S12 (BiSbTe-OAC system).

2 Theta (Degree)	Intensity	Phase	(h k l)
23.01	Very weak	Te (HEX)	(1 0 0)
27.57	Strong	Te (HEX), Bi ₂ Te ₃ (RHO)	(101), (015)
28.20	Medium	Sb ₂ Te ₃ (RHO)	(015)
37.89	Weak	Bi ₂ Te ₃ (RHO)	(1010)
38.24	Medium	Sb ₂ Te ₃ (RHO), Te(HEX)	(1010), (102)
40.43	Medium	Te (HEX)	(110)
41.03	Very weak	Bi ₂ Te ₃ (RHO)	(110)
42.62	Weak	Sb ₂ Te ₃ (RHO)	(110)
43.33	Weak	Te (HEX)	(111)
45.26	Very weak	Te (HEX)	(003)
45.86	Weak	Te(HEX), Sb ₂ Te ₃ (RHO)	(003), (1013)
47.03	Very weak	Te (HEX)	(200)
49.63	Weak	Te (HEX)	(201)
50.56	Very weak	Sb ₂ Te ₃ (RHO)	(119)
51.19	Very weak	Te (HEX)	(112)
51.97	Very weak	Sb ₂ Te ₃ (RHO)	(205)
56.84	Weak	Sb ₂ Te ₃ (RHO), Te (HEX)	(0117), (202)
58.35	Very weak	Sb ₂ Te ₃ (RHO)	(0210)

HEX=Hexagonal, RHO=Rhombohedral